Environmental Pollution 263 (2020) 114616

Contents lists available at ScienceDirect

Environmental Pollution

journal homepage: www.elsevier.com/locate/envpol

Determination of bisphenol A and bisphenol S by a covalent organic framework electrochemical sensor☆

Yue-Hong Pang *, Yu-Ying Huang , Li Wang , Xiao-Fang Shen , Yi-Ying Wang

State Key Laboratory of Food Science and Technology, School of Food Science and Technology, Jiangnan University, Wuxi, 214122, China

ARTICLE INFO

Article history:
Received 30 December 2019
Received in revised form
14 April 2020
Accepted 14 April 2020
Available online 18 April 2020

Keywords:
Covalent organic framework
Bisphenol A
Bisphenol S
Electrochemical sensor

ABSTRACT

Bisphenol A (BPA) is a widely produced chemical that is mainly used as raw material for manufacturing plastic products. It is an endocrine disruptor and causes irreversible damage to the human body. Bisphenol S (BPS), an alternative to BPA, has low dose effects on toxicology and genotoxicity. Herein, we constructed a highly porous crystalline covalent organic framework (COF, CTpPa-2)-modified glassy carbon electrode (GCE) for the electrochemical sensing of BPA and BPS. The electrochemical properties of the CTpPa-2/GCE were characterized using galvanostatic charge-discharge, cyclic voltammetry and differential pulse voltammetry. The CTpPa-2/GCE exhibited remarkable electrocatalytic activity, and the electrochemical responses for BPA and BPS were found to be linear in the concentration ranges of 0.1 −50 μM and 0.5−50 μM with detection limits of 0.02 μM and 0.09 μM (S/N = 3), respectively. Moreover, the fabricated sensor was utilized to determine BPA and BPS in bottle samples with recoveries of 87.0% −92.2% and migration rates of 13.2%−28.0%.

1. Introduction

Bisphenol A (BPA) is an industrial chemical that is widely used in the production of polycarbonate plastics, epoxy resins, and many consumer products, such as thermal paper and food containers (Chen et al., 2016; Liao and Kannan, 2018; Zhang et al., 2019; Zhou et al., 2019). However, BPA is also a well-known endocrine disruptor that is associated with various adverse health effects on sexual differentiation, brain development and immunologic function, especially for infants and children (Aker et al., 2016; Braun et al., 2017; Chen et al., 2018). In addition, it can migrate to food, beverages and drinking water under prolonged storage and elevated temperatures, eventually migrating to human beings (Yang et al., 2018). Due to concerns about widespread human exposure and potential harmful health effects, the European Union and China have implemented regulations and restrictions on the production and use of BPA (Kärrman-Toussaint et al., 2007; Migeot et al., 2013). Due to public concern and government regulations on BPA, bisphenol S (BPS), a kind of bisphenol analog with higher thermal stability and lower biodegradability, has been used as a BPA substitute in various applications (Wu et al., 2018). However, an increasing number of studies have shown that BPS has similar or higher adverse effects on androgen activity than BPA, and BPS has low dose effects on toxicology and genotoxicity (Héliès-Toussaint et al., 2014; Kinch et al., 2015; Rochester and Bolden, 2015; Rosenmai et al., 2014). Therefore, it is urgent to develop a rapid and simple method for the detection of BPA and BPS.

In recent years, the detection methods for BPA and BPS have mainly concentrated on high-performance liquid chromatography (Xiong et al., 2018; Zhang et al., 2019; Zhou et al., 2018) and gas chromatography (Fernandez et al., 2017; Mandrah et al., 2017; Wang et al., 2017). These methods can achieve higher accuracy and lower detection limits. However, complex sample pretreatment, expensive analytical cost and time-consuming nature are barriers to chromatography. Electrochemical sensors have the advantages of simple operation, low cost, high sensitivity and high efficiency. BPA and BPS have two electroactive phenolic hydroxyls, and the electrochemical method is expected to be an effective method to detect them (Ashraf et al., 2019; Zhu et al., 2016). The response signal of a typical bare electrode is very weak, which leads to poor recognition ability and insufficient determination. To solve these problems, different attempts have been made to modify electrodes with carbon nanotubes (Mo et al., 2019; Hoda and Mostafa, 2018), graphene (Reza et al., 2015), quantum dots (Rao et al., 2018; Yao et al., 2019), metal-organic frameworks (Lu et al., 2016) and hollow porous

☆ This paper has been recommended for acceptance by Charles Wong.

* Corresponding author.
E-mail address: yhpang@jiangnan.edu.cn (Y.-H. Pang).

https://doi.org/10.1016/j.envpol.2020.114616
0269-7491/

spherical Ni-loaded $CdFe_2O_4$ (Wang et al., 2017). However, it is still a challenge to find a suitable functional material to construct sensitive BPA and BPS electrochemical sensing platforms.

Nanomaterials are considered to be ideal materials for improving the sensitivity and selectivity of electrochemical sensors (Ben Messaoud et al., 2017; Butmee et al., 2019; Canevari et al., 2019). Framework materials can provide uniform nanometer-scale pores to organize functional building blocks (DeBlase et al., 2013). Covalent organic frameworks (COFs) represent an exciting new type of highly ordered porous crystalline structure constructed by strong covalent bonds between organic subunits (Qian et al., 2018; Wang et al., 2018; Zhao et al., 2017). Compared with conventional materials, COFs have the advantages of large specific surface area, good chemical and thermal stability, π conjugation, tunable porosity and low density, which make them potentially useful in diverse fields, including gas storage, photoconduction, catalysis and chromatography (Díaz and Corma, 2016; Huang et al., 2016; Rogge et al., 2017). In recent years, COFs have been gradually applied to the construction of electrochemical sensors (Zhang et al., 2019). Liang et al. and Yang et al. developed COF-based electrodes for electrochemical sensing of H_2O_2 (Liang et al., 2019; Yang et al., 2019). Ma et al. synthesized Zr-coordinated amide porphyrin-based two-dimensional COFs for electrochemical sensing of tetracycline (Ma et al., 2019). However, to the best of our knowledge, COF-based sensors have not been developed for the detection of bisphenols.

CTpPa-2, a COF that was synthesized by first functionalizing 1,3,5-triformylphloroglucinol (Tp) with chiral (+)-diacetyl-$_L$-tartaric anhydride to form the chiral functionalized monomer CTp; then, 2,5-dimethyl-p-phenylenediamine (Pa-2) was condensed with CTp to obtain COFs CTpPa-2 (Qian et al., 2016). The appropriate pore size (12 Å) and large π conjugated structure make CTpPa-2 potentially useful for the preconcentration of BPA and BPS (benzene homologues with theoretical molecular diameters of 9.6 Å for BPA and 10.0 Å for BPS) through the size matching effect and π-π stacking interaction. Herein, based on the size matching and π-π conjugation of CTpPa-2 toward BPA and BPS, an alternative electrode-modified material, namely, CTpPa-2, has been used to demonstrate the feasibility of COF-based electrochemical sensors for BPA and BPS and applied for real sample determination.

2. Experimental

2.1. Reagents and materials

BPA (99%), BPS (99%) and Nafion (a 5% by wt. solution in lower aliphatic alcohols and water) were purchased from J&K Chemical (Beijing, China). Catechol (99%) was obtained from Aladdin (Shanghai, China). Phosphate-buffered saline (PBS, 0.1 M) served as the supporting electrolyte and was prepared by mixing solutions of potassium hydrogen phosphate (K_2HPO_4) and potassium dihydrogen phosphate (KH_2PO_4) with the addition of sodium chloride (NaCl). CTpPa-2 was kindly provided by Professor Xiu-Ping Yan (College of Chemistry, Nankai University) based on their previous report (Qian et al., 2016). All reagents used were of analytical grade. Stock solutions of BPA and BPS (10.0 mM) were prepared by dissolving BPA and BPS in ethanol and kept at 4 °C in the darkness. The standard working solutions were freshly prepared by diluting the stock solution with 0.1 M PBS before use. All aqueous solutions were prepared by deionized water (18.2 MΩ·cm, 25 °C) obtained from a Milli-Q Integral Cabinet 3 system (Millipore, Bedford, USA).

2.2. Apparatus

All electrochemical measurements were performed using a CHI660C electrochemical workstation with a three-electrode system consisting of a modified glassy carbon working electrode (GCE, CH, d = 3 mm), a saturated calomel reference electrode and a platinum wire counter electrode (Chenhua Instrument, CH, Shanghai, China). The morphology of CTpPa-2 was recorded on a su8100 scanning electron microscope (SEM, Hitachi, Japan). The nitrogen adsorption-desorption isotherms were performed on an Autosorb-iQ analyzer (Quantachrome, USA). A pH meter (FE20K, Mettler-Toledo, Switzerland) was used to adjust the pH of the solutions. All measurements were carried out at room temperature.

2.3. Electrode modification

Before modification, the bare GCE was mechanically polished with alumina powder (3 μm and 0.05 μm), followed by ultrasonic rinsing with nitric acid (25%, v/v), ethanol and deionized water for 1 min in turn, and dried with nitrogen. A total of 5.0 mg CTpPa-2 was dispersed in 5.0 mL ethanol by ultrasonic treatment for 2 h, followed by the addition of 1% Nafion ethanol solution and ultrasonication to obtain a homogeneous suspension. Then, 5.0 μL CTpPa-2 suspension was dropped onto the GCE surface and exposed to air to evaporate the solvent. The modified CTpPa-2/GCE was rinsed carefully with deionized water and dried at room temperature.

2.4. Electrochemical measurement

The electrochemical analyses were performed via cyclic voltammetry (CV), galvanostatic charge-discharge (GCD) or differential pulse voltammetry (DPV). All solutions were deoxygenated by pumping with nitrogen for at least 15 min before measurements. CV was carried out at a scan rate of 100 mV s^{-1} in the range of 0−1.2 V. The GCD curves were recorded in 0.1 M PBS (pH = 7.0) within the potential of −0.4 V−0.8 V. DPV measurements were recorded in the potential range from 0.2 V to 1.0 V with a scan rate of 100 mV s^{-1}.

2.5. Pretreatment of bottle samples

Three kinds of bottle samples (mineral water bottle, polycarbonate bottle and baby bottle) were collected from the local supermarket. Before performing the simulated migration tests, bottle samples were cleaned with deionized water. The release of BPA and BPS from bottle samples was investigated using the overall filling method with acetonitrile up to the total volume. The bottles were immersed in a 60 °C water bath for 24 h, after which all the bottles were naturally cooled to room temperature. The acetonitrile extraction solution was then evaporated to almost dryness by a rotary evaporator. The extract was reconstituted with 20 mL of acetonitrile three times, and the extract was combined and stored in glass vials at 4 °C before analysis. A certain amount of sample was diluted with PBS, and then, the standard addition method was used for quantitative analysis of BPA and BPS.

3. Results and discussion

3.1. Design of a COF-based electrochemical sensor for the detection of BPA and BPS

The CTpPa-2/GCE application for electrochemical sensing of BPA and BPS is shown in Fig. 1. Two-dimensional porous crystalline imine-linked COF CTpPa-2 with excellent stability and large π conjugated structure is ideally suited for conjugate accumulation (Bunck and Dichtel, 2013; Kandambeth et al., 2012; Qian et al., 2016). BPA and BPS are benzene homologues with theoretical

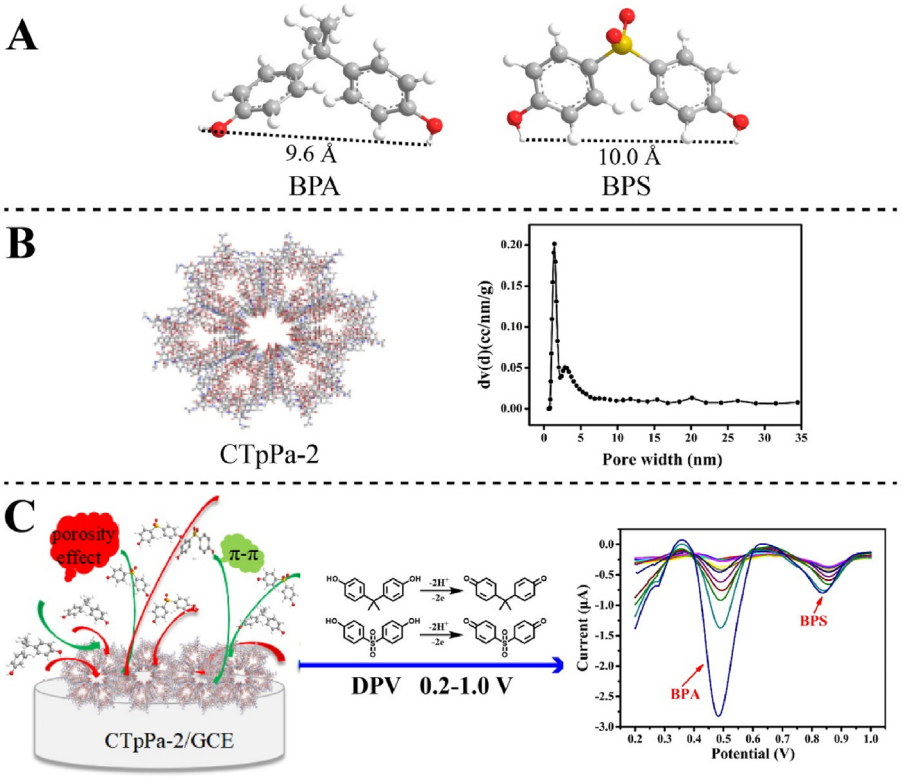

Fig. 1. (A) The structures of BPA and BPS; (B) The extended structure and pore size distribution of CTpPa-2; (C) Electrochemical response and the possible electrochemical oxidation mechanism of BPA and BPS on the CTpPa-2/GCE.

molecular diameters (9.6 Å for BPA and 10.0 Å for BPS) (Fig. 1A). The appropriate pore size of CTpPa-2 (12 Å) and large π-conjugated structure facilitate the accumulation of BPA and BPS via π-π conjugate aggregation and porosity effects (Fig. 1B). Meanwhile, BPA and BPS are negatively charged, and the accumulation potential of +0.3 V for 70 s was chosen for the electrostatic attraction accumulation. The accumulated bisphenols were electrooxidized to the corresponding quinine by $2H^+$ and $2e^-$ participation in the electrode-solution interface (Dhanjai et al., 2018), and the proposed oxidation mechanism of BPA and BPS is presented in Fig. 1C. Scanning DPV in the range of 0.2 V–1.0 V, two well-defined and easily distinguishable anodic current signals were obtained as the analytical signals to determine for BPA and BPS (Fig. 1C).

3.2. Electrochemical properties of CTpPa-2/GCE

The electrochemical capacitance properties of CTpPa-2 were investigated by the GCD method at different current densities. The GCD curves of the CTpPa-2/GCE at several current densities within the potential of −0.4 V to 0.8 V are shown in Fig. 2A and B. The charge-discharge time and specific capacitance decrease with increasing current density, and the coulombic efficiency remains above 71%. The specific capacitance of CTpPa-2 is 325 F g^{-1} at a current density of 0.4 A g^{-1}, which is higher than that of activated carbon (Wang et al., 2019), OMS-2 (Cao et al., 2012) and nanostructured polyanilines (Li et al., 2015).

The CVs of the bare GCE and the CTpPa-2-modified electrodes in 1.0 mM $[Fe(CN)_6]^{3-}/[Fe(CN)_6]^{4-}$ (+0.2 M KCl) at a scan rate of 100 mV s^{-1} are shown in Fig. 2C. A pair of quasi-reversible redox peaks are obtained, and the redox peak current of the Fe^{2+}/Fe^{3+} redox couple at the CTpPa-2/GCE (−52.23 μA and 49.20 μA) is slightly higher than that at the bare GCE (−45.61 μA and 42.94 μA). The electrochemical active surface area of the modified electrode is calculated based on the Randles-Sevcik equation (Rao et al., 2018)

$$I_p = 268600n^{3/2}AD^{1/2}Cv^{1/2}$$

where I_p is the anodic peak current (A), and n is the electron transfer number of the redox event (n = 1). *A* is the active surface area of the modified electrode, D is the diffusion coefficient of ferricyanide (D = 7.60 × 10^{-6} cm^2 s^{-1}) (Nouri et al., 2019), C is the concentration of $[Fe(CN)_6]^{3-}/[Fe(CN)_6]^{4-}$ (mol cm^{-3}), and *v* is the scan rate (V s^{-1}). The value of the electrochemical active surface area correspondingly obtained for the CTpPa-2/GCE is calculated to be 0.233 cm^2, which is higher than that of the bare GCE (0.195 cm^2). CTpPa-2/GCE has a large specific capacitance and an increased electrochemical active surface area, which lead to good electron transfer and conductivity. The stability of CTpPa-2 was characterized by 1500 charge-discharge cycles at a current density of 0.8 A g^{-1} (Fig. 2D). The results show that after 1500 cycles of GCD, the specific capacitance of CTpPa-2 is still 84% retention, indicating that CTpPa-2 has good stability.

3.3. Electrochemical performances of BPA and BPS

The morphologies of the bare GCE and the CTpPa-2/GCE were observed by SEM (Fig. 3A and B). Compared with the smooth bare GCE, the surface of the CTpPa-2/GCE is crumpled and flocculent, which provides it with a larger specific surface area and more effective π-electron system. The difference in electrochemical performances between bare GCE and CTpPa-2/GCE was observed by the CV method (Fig. 3C). Neither bare GCE (a) nor CTpPa-2/GCE (b) show redox peaks of BPA and BPS in 0.1 M PBS (pH = 7.0), while two oxidation peaks are observed in the presence of BPA and BPS (c

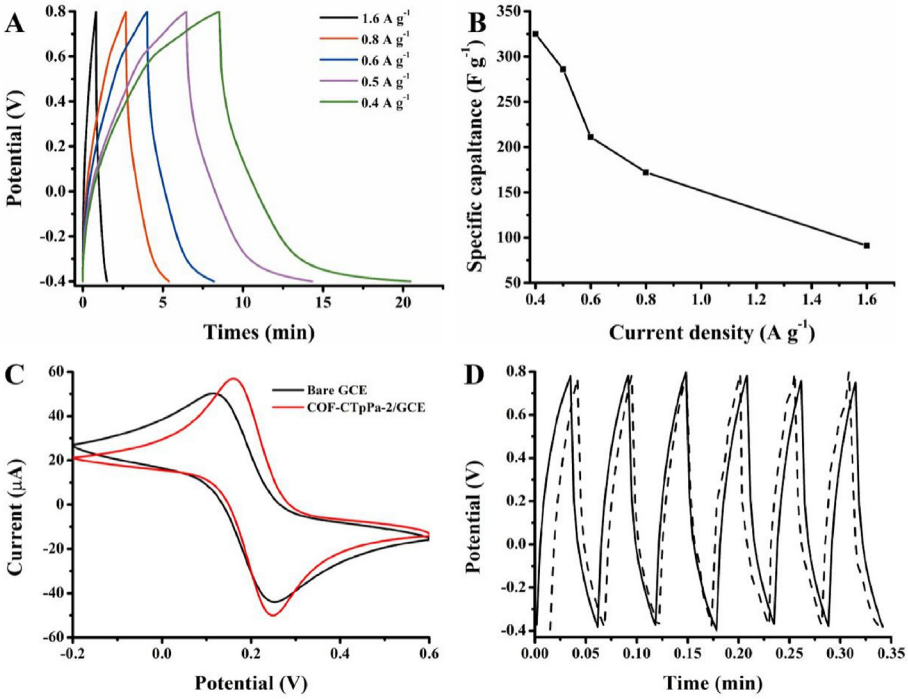

Fig. 2. (A) GCD of CTpPa-2 at current densities between 0.4 A g^{-1} and 1.6 A g^{-1} in 0.1 M PBS (pH 7.0); (B) Specific capacitance of CTpPa-2 at varying current densities; (C) CV of bare GCE and CTpPa-2/GCE in 1.0 mM $[Fe(CN)_6]^{3-}/[Fe(CN)_6]^{4-}$ (+0.2 M KCl) at a scan rate of 100 mV s^{-1}; (D) Long-term cyclic stability performance at a current density of 0.8 A g^{-1} of the GCD experiment (Solid-line: 1st–6th; dashed line: 1495th–1500th).

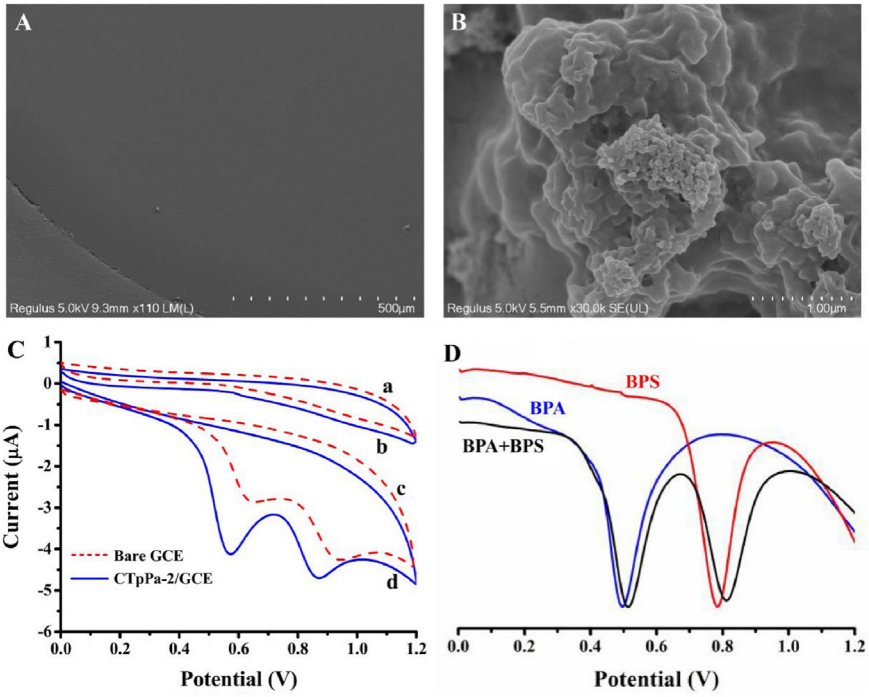

Fig. 3. SEM images of (A) bare GCE and (B) CTpPa-2/GCE; (C) CV of bare GCE and CTpPa-2/GCE in 0.1 M PBS (pH 7.0) (a, b) and in 0.1 M PBS containing 40 μM BPA and BPS (c, d); (D) DPV curve of 40 μM BPA, BPS and their mixture in PBS (pH 7.0) at CTpPa-2/GCE. Scan rate: 100 mV s^{-1}.

and d), indicating that the electrochemical reactions of BPA and BPS on the electrode are irreversible. Moreover, the oxidation peak currents of BPA and BPS at CTpPa-2/GCE are larger than those at bare GCE, which may be due to the synergistic effect of π-π conjugation and porosity effect, so that CTpPa-2 has an excellent enrichment effect on BPA and BPS. DPV was applied to investigate the CTpPa-2/GCE for determination of BPA and BPS (Fig. 3D). The oxidation peaks for BPS and BPA are at +0.794 V and +0.496 V, respectively. In the mixture of BPS and BPA, their DPVs show two well-defined sharp oxidation peaks with potentials of +0.812 V

and +0.512 V, respectively. Appropriate peak-peak potential separation (ΔE_p, 0.300 V) is large enough for the detection of BPA and BPS.

The effect of scan rate on the electrochemical oxidation of BPA and BPS at CTpPa-2/GCE was measured by CV (Fig. 4). The oxidation peak currents (I_{pa}) of BPA and BPS increase with increasing scan rate (υ) from 10 to 100 mV s^{-1} (Fig. 4A and B). The linear relationship between I_{pa} and υ is $I_{pa} = -15.41\upsilon - 0.563$ ($R^2 = 0.999$) for BPS and $I_{pa} = -15.48\upsilon - 0.534$ ($R^2 = 0.999$) for BPA, indicating that BPA and BPS at CTpPa-2/GCE are typical adsorption-controlled electrochemical processes.

In addition, the oxidation peak potentials (E_{pa}) of BPA and BPS show a logarithmic relationship with the scan rate (Fig. 4D). Based on the irreversible adsorption-controlled processes, E_{pa} can be defined by the following equation on the basis of Laviron's theory (Laviron, 1974):

$$E_{pa} = E^0 + \frac{RT}{\alpha nF}\ln\frac{RTk_s}{\alpha nF} + \frac{RT}{\alpha nF}\ln\upsilon$$

where E^0 refers to the formal redox potential, R is the gas constant (R = 8.314), T is the absolute temperature (T = 298 K), α is the transfer coefficient and assumed to be 0.5 in the irreversible electrode process, F is the Faraday constant (F = 96,485 C mol^{-1}), and k_s is the standard rate constant. According to the linear correlation between E_{pa} and lnυ, the slope is equal to RT/αnF. Combined with the above data, the electron transfer number (n) of both BPA and BPS is calculated to be approximately 2. It is further confirmed that $2H^+$ and $2e^-$ of BPA and BPS participate in electrooxidation at the electrode solution interface.

3.4. Optimization of analytical conditions

The effect of pH in the range of 4.0–9.0 at CTpPa-2/GCE for BPA and BPS was investigated (Fig. 5A and B). The E_{pa} values of BPA and BPS shift negatively with increasing pH, indicating that protons are involved in the electrochemical reaction. According to the linear relationship between E_{pa} and pH (inset of Fig. 5A), the slopes for BPA and BPS are −56 mV/pH and −55 mV/pH, respectively, which are close to the theoretical value of −58 mV/pH. According to the Nernst equation, electron transfer is accompanied by an equal number of protons in the electrode reaction. Because the electron transfer number of BPA and BPS is 2, the electrochemical reaction of BPA and BPS involves a two-electron and two-proton transfer process. The peak currents increase gradually with increasing pH and reach a maximum at a pH of 7.0. Thus, a pH of 7.0 was chosen for the following experiments.

The response of BPA increases as the accumulation potential increases from −0.3 V to 0.2 V, and then, the response began to decrease slightly with increasing potential. The response of BPS is similar, reaching a maximum at a potential of 0.3 V (Fig. 5C). Therefore, 0.3 V was used as the optimal accumulation potential for further experiments. For accumulation time, the peak currents of BPA increase gradually until 70 s and then remain steady, and the response currents of BPS enter the stable stage after 60 s (Fig. 5D). Therefore, we chose 70 s as the accumulation time in the following experiment.

3.5. Quantitative analysis of BPA and BPS

DPV was carried out for the determination of BPA and BPS in the range of 0.2 V–1.0 V with 100 mV s^{-1} in 0.1 M PBS (pH = 7) after accumulation on the CTpPa-2/GCE for 70 s at a constant potential of 0.3 V. For quantitatively analyzing BPA, the concentration of BPS was fixed at 3.0 μM. As the BPA concentration increased, the response current of BPA was proportional to the concentration in the range of 0.1–50 μM with two linear relationships, while that of BPS remained essentially unchanged (Fig. 6A and B). The regression equation was I_{pa} (μA) = $-0.1263C_{BPA} - 0.0135$ ($R^2 = 0.994$) at low concentrations (0.1–2.5 μM) and I_{pa} (μA) = $-0.0501C_{BPA} - 0.2249$ ($R^2 = 0.997$) at high concentrations (2.5–50 μM). Similarly, the CTpPa-2/GCE displayed two linear responses in the BPS concentration ranges of 0.5–8.0 μM and 8.0–50 μM in the presence of

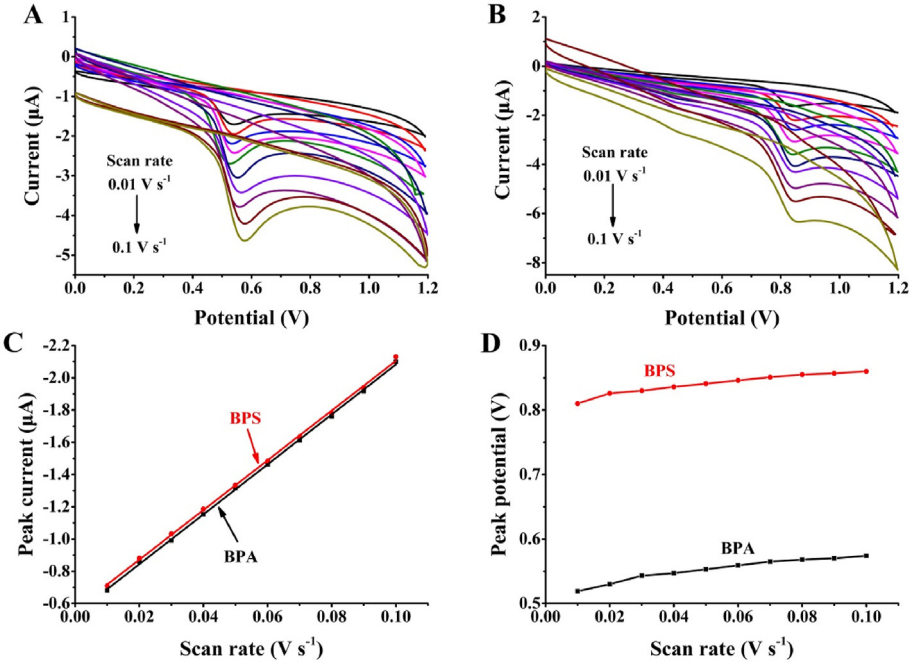

Fig. 4. CV of 40 μM (A) BPA and (B) BPS on CTpPa-2/GCE at different scan rates (10–100 mV s^{-1}); Relationship between the (C) oxidation peak current and the (D) oxidation peak potential of BPS and BPA with scan rates.

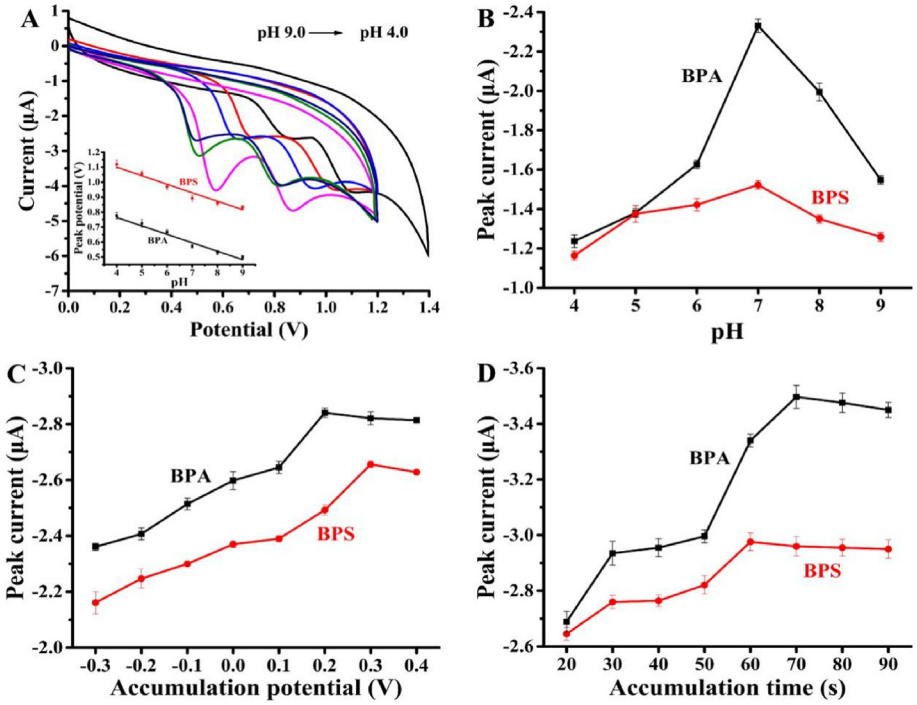

Fig. 5. (A) CV of 40 μM BPA and BPS in 0.1 M PBS with different pH values (4.0–9.0) on the CTpPa-2/GCE at a scan rate of 100 mV s^{-1}, insert shows the relationship between the oxidation peak potential and pH. Effect of experimental conditions on electrochemical response: (B) pH, (C) accumulation potential and (D) accumulation time of 40 μM BPA and BPS on the CTpPa-2/GCE.

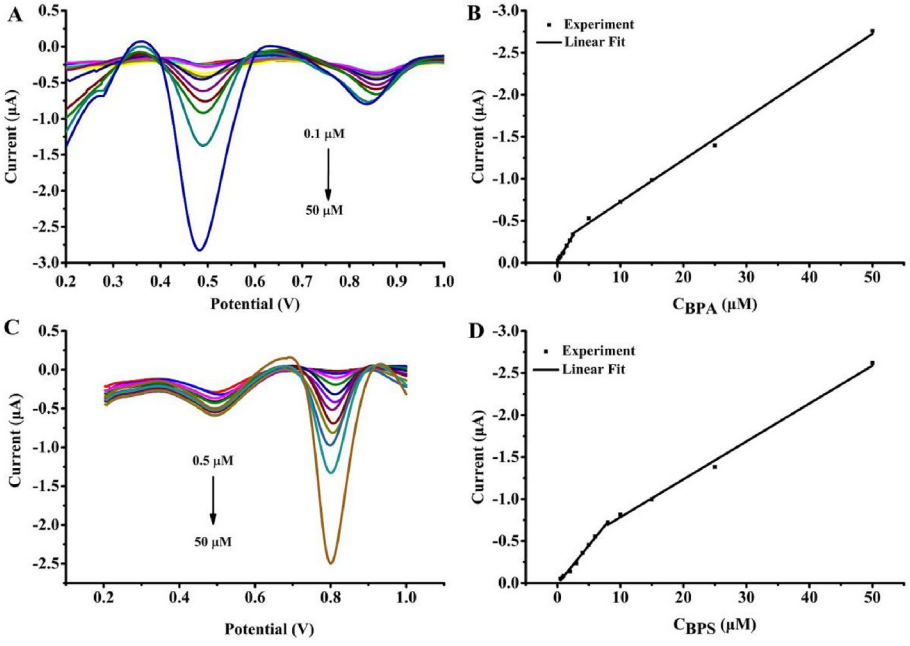

Fig. 6. (A) DPV on the CTpPa-2/GCE in 0.1 M PBS (pH 7.0) containing 3.0 μM BPS and different concentrations of BPA (0.1, 0.3, 0.5, 0.8, 1.0, 1.5, 2.0, 2.5, 5.0, 10.0, 15.0, 25.0, 50.0 μM); (B) Calibration plot of peak current versus BPA concentrations; (C) DPV on the CTpPa-2/GCE in 0.1 M PBS (pH 7.0) containing 3.0 μM BPA and different concentrations of BPS (0.5, 0.8, 1.0, 2.0, 3.0, 4.0, 5.0, 6.0, 8.0, 10.0, 15.0, 25.0, 50.0 μM); (D) Calibration plot of peak current versus BPS concentrations.

3.0 μM BPA (Fig. 6C and D), which can be expressed as I_{pa} (μA) = $-0.0923C_{BPS} + 0.0130$ ($R^2 = 0.990$) at low concentrations (0.5–8.0 μM) and I_{pa} (μA) = $-0.0451C_{BPS} - 0.3324$ ($R^2 = 0.996$) at high concentrations (8.0–50 μM). The detection limits were calculated as 0.02 μM for BPA and 0.09 μM for BPS (S/N = 3).

The analytical performances of different electrochemical methods for the determination of BPA and BPS are presented in Table 1. Compared to previously reported sensors for the detection of BPA and BPS (Lin et al., 2014; Zhu et al., 2014; Zhu et al., 2016; Zheng et al., 2016; Wang, 2018; Yao et al., 2019; Butmee et al., 2019; Mo et al., 2019; Wang et al., 2015; Lu et al., 2016; Ling et al., 2018), our proposed sensor has a lower detection limit and a comparable

Table 1
Comparison of the proposed method with other previously reported electrochemical methods for the determination of BPA and BPS.

Modified electrode	Analyte	Linear Range (μM)	Detection Limit (μM)	References
Polyglutamic acid/amino-functionalized carbon nanotubes nanocomposite	BPA	0.1–10	0.02	Lin et al. (2014)
Magnetic molecularly imprinted nanoparticles	BPA	0.6–100	0.1	Zhu et al. (2014)
Electrochemically co-reduced 3D GO-C_{60} nanoassembly	BPS	1–100	0.5	Zhu et al. (2016)
Platinum/poly(diallyl dimethyl ammonium chloride)-diamond powder hybrid	BPA	5–30	0.6	Zheng et al. (2016)
	BPS	10–60	2.0	
Multiwalled carbon nanotubes	BPA	2–30	0.5	Wang, (2018)
	BPS	20–80	4.0	
Molecularly imprinted polymer and B,N,F-CQDs/AgNPs	BPS	0.01–50	0.112	Yao et al. (2019)
Ionic liquid functionalized graphene nanoplatelets	BPA	0.02–5.0	6.4	Butmee et al. (2019)
AuPd incorporated carboxylic multiwalled carbon nanotubes	BPA	0.18–18	60	Mo et al. (2019)
Copper-centered metal-organic framework (MOF)	BPA	0.05–3.0	0.013	Wang et al. (2015)
CuMOF-based tyrosinase	BPA	0.05–3.0	0.013	Lu et al. (2016)
Amine-functionalized MOF/reduced graphene oxide composites	BPA	2–200	0.7966	Ling et al. (2018)
Covalent organic framework CTpPa-2	BPA	0.1–50	0.02	This work
	BPS	0.5–50	0.09	

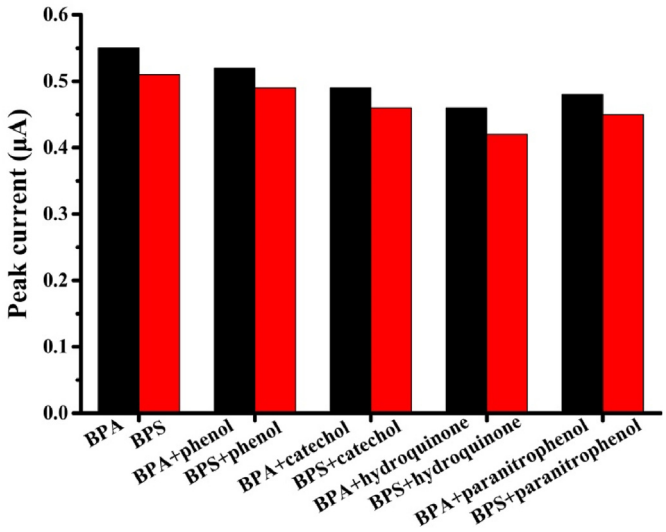

Fig. 7. Comparison of the current response of CTpPa-2/GCE with 5 μM BPA and BPS in the absence or presence of 5 μM other phenolic compounds (phenol, catechol, p-nitrophenol and hydroquinone).

or better wider linear range, indicating that the electrochemical sensor based on the covalent organic framework CTpPa-2 is a good candidate for the sensitive detection of BPA and BPS.

3.6. Reproducibility, stability and interference

The reproducibility, stability and interference were investigated to evaluate the sensor performance. Six CTpPa-2/GCEs were prepared simultaneously by means of the same procedure, and the relative standard deviation (RSD) was calculated to be 4.8% for BPA and 5.1% for BPS. In addition, the prepared modified electrode retained 92.1% (BPA) and 89.5% (BPS) of the original response after being stored in a refrigerator at 4 °C for two weeks. To further verify the selectivity of the CTpPa-2/GCE to BPA and BPS, five phenolic compounds (phenol, catechol, p-nitrophenol and hydroquinone) were selected as the interferents. As shown in Fig. 7, it is found that the equivalent phenolic compounds (phenol, catechol, p-nitrophenol and hydroquinone) have little effect on the performance of CTpPa-2/GCE for the determination of BPA and BPS, and the proposed electrode maintains more than 86.0% of the initial response to BPA and BPS. Moreover, a 100-fold concentration of inorganic ions (Cu^{2+}, Ca^{2+}, Cl^{-}, NO_3^{-}, Mg^{2+}, K^{+}, SO_4^{2-}) also had no influence on the signals of BPA and BPS with deviations below 5.0%. These results demonstrate that CTpPa-2/GCE has good reproducibility, stability and anti-interference ability for the determination of BPA and BPS.

3.7. Real sample analysis

The as-fabricated CTpPa-2/GCE sensor was used to determine BPA and BPS in three commercial plastic products (mineral water bottle, polycarbonate bottle and baby bottle), and the results are presented in Table 2. The contents of BPA and BPS in baby bottles were lower than the detection limit. The concentration of BPA was 0.52 μM in polycarbonate bottles and 2.03 μM in mineral water bottles. For BPS, the concentration of the polycarbonate bottle was 0.46 μM, and that of the mineral water bottle was 1.26 μM. To assess the accuracy of the sensor, plastic bottles were spiked with BPA and BPS at a certain concentration, and recoveries were achieved in the range of 87.0%–91.0% for BPA and 89.6%–92.2% for BPS; the RSDs were within 2.2%–6.5% (n = 3). The results show that the proposed method is feasible for the detection of BPA and BPS in real samples.

The migration of BPA and BPS from bottle samples to food was investigated by detecting simulant aqueous food (water) in a 60 °C

Table 2
Determination of BPA and BPS in real samples (n = 3).

Samples	Spiked (μM)	BPA			Spiked (μM)	BPS		
		Found (μM)	RSD (%)	Recovery (%)		Found (μM)	RSD (%)	Recovery (%)
Mineral water bottle	–	2.03	4.5	–	–	1.26	1.1	–
	0.1	2.12	2.3	87.0	0.5	1.72	4.2	92.2
Polycarbonate bottle	–	0.52	2.9	–	–	0.46	2.8	–
	0.1	0.61	5.2	90.0	0.5	0.91	5.7	89.6
Baby bottle	–	nd[a]	–	–	–	nd	–	–
	0.1	0.09	6.5	91.0	0.5	0.45	2.2	90.6

[a] Not detected.

bath for 24 h. The migration percentage was defined as:

$$\text{Migration rate}(\%) = \frac{C_{\text{BPA or BPS}} \text{ in simulant}}{C_{\text{BPA or BPS}} \text{ in bottle}} \times 100\%$$

The migration rates of BPA and BPS in mineral water bottles were 22.1% and 13.2%, respectively, and those in polycarbonate bottles were 28.0% and 26.0%, respectively.

4. Conclusion

In summary, an electrochemical sensor based on the functional material CTpPa-2 has been constructed for the determination of BPA and BPS. The sensor has an acceptable wide linear range and a low detection limit with satisfactory repeatability, selectivity and stability. In addition, the proposed method has been successfully applied to the determination of BPA and BPS in practical samples, which indicates that the COF-based electrochemical sensor is acceptable for use in environmental analysis and food safety.

Declaration of competing interest

The authors declare that they have no known competing financial interests or personal relationships that could have appeared to influence the work reported in this paper.

CRediT authorship contribution statement

Yue-Hong Pang: Conceptualization, Resources, Writing - review & editing, Project administration, Funding acquisition. **Yu-Ying Huang:** Conceptualization, Methodology, Formal analysis, Investigation, Writing - original draft. **Li Wang:** Validation, Investigation, Data curation. **Xiao-Fang Shen:** Methodology, Formal analysis, Validation, Investigation. **Yi-Ying Wang:** Conceptualization, Methodology, Investigation.

Acknowledgments

This work was supported by the National Natural Science Foundation of China (21976070), National Key R&D Program of China (2018YFC1604202), and the Fundamental Research Funds for the Central Universities (JUSRP22003). We also thank Professor Xiu-Ping Yan for their COFs materials and valuable discussions.

Appendix A. Supplementary data

Supplementary data to this article can be found online at https://doi.org/10.1016/j.envpol.2020.114616.

References

Aker, A.M., Watkins, D.J., Johns, L.E., Ferguson, K.K., Soldin, O.P., Anzalota Del Toro, L.V., Alshawabkeh, A.N., Cordero, J.F., Meeker, J.D., 2016. Phenols and parabens in relation to reproductive and thyroid hormones in pregnant women. Environ. Res. 151, 30–37.

Ashraf, G., Asif, M., Aziz, A., Wang, Z., Qiu, X., Huang, Q., Xiao, F., Liu, H., 2019. Nanocomposites consisting of copper and copper oxide incorporated into MoS4 nanostructures for sensitive voltammetric determination of bisphenol A. Mikrochim. Acta 186, 337.

Ben Messaoud, N., Ghica, M.E., Dridi, C., Ben Ali, M., Brett, C.M.A., 2017. Electrochemical sensor based on multiwalled carbon nanotube and gold nanoparticle modified electrode for the sensitive detection of bisphenol A. Sensor. Actuator. B Chem. 253, 513–522.

Braun, J.M., Yolton, K., Stacy, S.L., Erar, B., Papandonatos, G.D., Bellinger, D.C., Lanphear, B.P., Chen, A., 2017. Prenatal environmental chemical exposures and longitudinal patterns of child neurobehavior. Neurotoxicology 62, 192–199.

Bunck, D.N., Dichtel, W.R., 2013. Postsynthetic functionalization of 3D covalent organic frameworks. Chem. Commun. 49, 2457–2459.

Butmee, P., Tumcharern, G., Saejueng, P., Stankovic, D., Ortner, A., Jitcharoen, J., Kalcher, K., Samphao, A., 2019. A direct and sensitive electrochemical sensing platform based on ionic liquid functionalized graphene nanoplatelets for the detection of bisphenol A. J. Electroanal. Chem. 833, 370–379.

Canevari, T.C., Rossi, M.V., Alexiou, A.D.P., 2019. Development of an electrochemical sensor of endocrine disruptor bisphenol A by reduced graphene oxide for incorporation of spherical carbon nanoparticles. J. Electroanal. Chem. 832, 24–30.

Cao, F., Liu, Y., Chen, B., Fei, L., Wanga, Y., Yuan, J., 2012. Enhancement of electrochemical capacitive properties based on complementation of morphologies. Electrochim. Acta 81, 1–7.

Chen, D., Kannan, K., Tan, H., Zheng, Z., Feng, Y.L., Wu, Y., Widelka, M., 2016. Bisphenol analogues other than BPA: environmental occurrence, human exposure, and toxicity-A review. Environ. Sci.Technol. 50, 5438–5453.

Chen, Y., Fang, J., Ren, L., Fan, R., Zhang, J., Liu, G., Zhou, L., Chen, D., Yu, Y., Lu, S., 2018. Urinary bisphenol analogues and triclosan in children from south China and implications for human exposure. Environ. Pollut. 238, 299–305.

DeBlase, C.R., Silberstein, K.E., Truong, T.T., Abruña, H.D., Dichtel, W.R., 2013. β-Ketoenamine-linked covalent organic frameworks capable of pseudocapacitive energy storage. J. Am. Chem. Soc. 135, 16821–16824.

Dhanjai, Sinha A., Wu, L., Lu, X., Chen, J., Jain, R., 2018. Advances in sensing and biosensing of bisphenols: a review. Anal. Chim. Acta 998, 1–27.

Díaz, U., Corma, A., 2016. Ordered covalent organic frameworks, COFs and PAFs. From preparation to application. Coord. Chem. Rev. 311, 85–124.

Fernandez, M.A.M., Andre, L.C., Cardeal, Z.L., 2017. Hollow fiber liquid-phase microextraction-gas chromatography-mass spectrometry method to analyze bisphenol A and other plasticizer metabolites. J. Chromatogr. A 1481, 31–36.

Héliès-Toussaint, C., Peyre, L., Costanzo, C., Chagnon, M.C., Rahmani, R., 2014. Is bisphenol S a safe substitute for bisphenol A in terms of metabolic function? An *in vitro* study. Toxicol. Appl. Pharmacol. 280, 224–235.

Hoda, E., Mostafa, R., 2018. Electrochemical behavior of the endocrine disruptor bisphenol A and in situ investigation of its interaction with DNA. Sensor. Actuator. B Chem. 274, 370–380.

Huang, N., Wang, P., Jiang, D., 2016. Covalent organic frameworks: a materials platform for structural and functional designs. Nat. Rev. Mater. 1, 1–19.

Kandambeth, S., Mallick, A., Lukose, B., Mane, M.V., Heine, T., Banerjee, R., 2012. Construction of crystalline 2D covalent organic frameworks with remarkable chemical (acid/base) stability via a combined reversible and irreversible route. J. Am. Chem. Soc. 134, 19524–19527.

Kärrman-Toussaint, A., Ericson, I., Bavel, B., Darnerud, P.O., Aune, M., Glynn, A., Lignell, S., Lindström, G., 2007. Exposure of perfluorinated chemicals through lactation: levels of matched human milk and serum and a temporal trend, 1996-2004, in Sweden. Environ. Health Perspect. 115, 226–230.

Kinch, C.D., Ibhazehiebo, K., Jeong, J.H., Habibi, H.R., Kurrasch, D.M., 2015. Low-dose exposure to bisphenol A and replacement bisphenol S induces precocious hypothalamic neurogenesis in embryonic zebrafish. Proc. Natl. Acad. Sci. U.S.A. 112, 1475–1480.

Laviron, E., 1974. Adsorption, autoinhibition and autocatalysis in polarography and in linear potential sweep voltammetry. J. Electroanal. Chem. 52, 355–393.

Li, T., Qin, Z., Liang, B., Tian, F., Zhao, J., Liu, N., Zhu, M., 2015. Morphology-dependent capacitive properties of three nanostructured polyanilines through interfacial polymerization in various acidic media. Electrochim. Acta 177, 343–351.

Liang, H., Xu, M., Zhu, Y., Wang, L., Xie, Y., Song, Y., Wang, L., 2019. H_2O_2 ratiometric electrochemical sensors based on nanospheres derived from ferrocence-modified covalent organic frameworks. ACS Appl. Nano Mater. 3 (1), 555–562.

Liao, C., Kannan, K., 2018. Species-specific accumulation and temporal trends of bisphenols and benzophenones in mollusks from the Chinese Bohai Sea during 2006-2015. Sci. Total Environ. 653, 168–175.

Lin, Y., Liu, K., Liu, C., Yin, L., Kang, Q., Li, L., Li, B., 2014. Electrochemical sensing of bisphenol A based on polyglutamic acid/amino-functionalised carbon nanotubes nanocomposite. Electrochim. Acta 133, 492–500.

Ling, L., Xu, J., Deng, Y., Peng, Q., Chen, J., San, H., Nie, Y., 2018. One-pot hydrothermal synthesis of amine-functionalized metal–organic framework/reduced graphene oxide composites for the electrochemical detection of bisphenol A. Anal. Methods 10 (23), 2722–2730.

Lu, X., Wang, X., Wu, L., Wu, L., Dhanjai, Fu L., Gao, Y., Chen, J., 2016. Response characteristics of bisphenols on a metal-organic framework-based tyrosinase nanosensor. ACS Appl. Mater. Interfaces 8, 16533–16539.

Ma, X., Pang, C., Li, S., Xiong, Y., Li, J., Luo, J., Yang, Y., 2019. Synthesis of Zr-coordinated amide porphyrin-based two-dimensional covalent organic framework at liquid-liquid interface for electrochemical sensing of tetracycline. Biosens. Bioelectron. 146, 111734.

Mandrah, K., Satyanarayana, G.N.V., Roy, S.K., 2017. A dispersive liquid-liquid microextraction based on solidification of floating organic droplet followed by injector port silylation coupled with gas chromatography-tandem mass spectrometry for the determination of nine bisphenols in bottled carbonated beverages. J. Chromatogr. A 1528, 10–17.

Migeot, V., Dupuis, A., Cariot, A., Albouy-Llaty, M., Pierre, F., Rabouan, S., 2013. Bisphenol A and its chlorinated derivatives in human colostrum. Environ. Sci.Technol. 47, 13791–13797.

Mo, F., Xie, J., Wu, T., Liu, M., Zhang, Y., Yao, S., 2019. A sensitive electrochemical sensor for bisphenol A on the basis of the AuPd incorporated carboxylic multi-walled carbon nanotubes. Food Chem. 292, 253–259.

Nouri, M., Rahimnejad, M., Najafpour, G., Akbar, M.A., 2019. A Gr/αFe_2O_3/Carbon paste electrode developed as an electrochemical sensor for determination of rizatriptan benzoate: an antimigraine drug. ChemistrySelect 4 (46), 13421–13426.

Qian, H.L., Yang, C.X., Wang, W.L., Yang, C., Yan, X.P., 2018. Advances in covalent organic frameworks in separation science. J. Chromatogr. A 1542, 1–18.
Qian, H.L., Yang, C.X., Yan, X.P., 2016. Bottom-up synthesis of chiral covalent organic frameworks and their bound capillaries for chiral separation. Nat. Commun. 7, 12104.
Rao, H., Zhao, X., Liu, X., Zhong, J., Zhang, Z., Zou, P., Jiang, Y., Wang, X., Wang, Y., 2018. A novel molecularly imprinted electrochemical sensor based on graphene quantum dots coated on hollow nickel nanospheres with high sensitivity and selectivity for the rapid determination of bisphenol S. Biosens. Bioelectron. 100, 341–347.
Reza, K.K., Ali, M.A., Srivastava, S., Agrawal, V.V., Biradar, A.M., 2015. Tyrosinase conjugated reduced graphene oxide based biointerface for bisphenol A sensor. Biosens. Bioelectron. 74, 644–651.
Rochester, J.R., Bolden, A.L., 2015. Bisphenol S and F: a systematic review and comparison of the hormonal activity of bisphenol A substitutes. Environ. Health Perspect. 123, 643–650.
Rogge, S.M.J., Bavykina, A., Hajek, J., Garcia, H., Olivos-Suarez, A.I., Sepúlveda-Escribano, A., Vimont, A., Clet, G., Bazin, P., Kapteijn, F., Daturi, M., Ramos-Fernandez, E.V., Xamena, F.X.L., Speybroeck, V.V., Gascon, J., 2017. Metal-organic and covalent organic frameworks as single-site catalysts. Chem. Soc. Rev. 46, 3134–3184.
Rosenmai, A.K., Dybdahl, M., Pedersen, M., Vugt-Lussenburg, B.M.A., Wedebye, E.B., Taxvig, C., Vinggaard, A.M., 2014. Are structural analogues to bisphenol A safe alternatives? Toxicol. Sci. 139, 35–47.
Wang, J., Li, J., Gao, M., Zhang, X., 2018. Recent advances in covalent organic frameworks for separation and analysis of complex samples. Trac. Trends Anal. Chem. 108, 98–109.
Wang, Q., Zhang, D., Yang, L., Zhang, L., 2017a. Constructed ILs@ hollow porous spherical Ni-loaded $CdFe_2O_4$ modified electrode for highly sensitive simultaneous electrochemical analysis of bisphenols. Sensor. Actuator. B Chem. 246, 800–808.
Wang, Q., Zhu, L., Chen, M., Ma, X., Wang, X., Xia, J., 2017b. Simultaneously determination of bisphenol A and its alternatives in sediment by ultrasound-assisted and solid phase extractions followed by derivatization using GC-MS. Chemosphere 169, 709–715.
Wang, X., 2018. Simultaneous determination of bisphenol A and bisphenol S using multi-walled carbon nanotubes modified electrode. Int. J. Electrochem. Sci. 13, 11906–11922.
Wang, X., Lu, X., Wu, L., Chen, J., 2015. 3D metal-organic framework as highly efficient biosensing platform for ultrasensitive and rapid detection of bisphenol A. Biosens. Bioelectron. 65, 295–301.
Wang, Y., Chang, Z., Qian, M., Zhang, Z., Lin, J., Huang, F., 2019. Enhanced specific capacitance by a new dual redox-active electrolyte in activated carbon-based supercapacitors. Carbon 143, 300–308.
Wu, L.H., Zhang, X.M., Wang, F., Gao, C.J., Chen, D., Palumbo, J.R., Guo, Y., Zeng, E.Y., 2018. Occurrence of bisphenol S in the environment and implications for human exposure: a short review. Sci. Total Environ. 615, 87–98.
Xiong, L., Yan, P., Chu, M., Gao, Y.Q., Li, W.H., Yang, X.L., 2018. A rapid and simple HPLC-FLD screening method with QuEChERS as the sample treatment for the simultaneous monitoring of nine bisphenols in milk. Food Chem. 244, 371–377.
Yang, D., Li, G., Wu, L., Yang, Y., 2018. Ferrofluid-based liquid-phase microextraction: analysis of four phenolic compounds in milks and fruit juices. Food Chem. 261, 96–102.
Yang, Y., Shen, Y., Wang, L., Song, Y., Wang, L., 2019. Three-dimensional porous carbon/covalent-organic framework films integrated electrode for electrochemical sensors. J. Electroanal. Chem. 855, 113590.
Yao, J., Chen, M., Li, N., Liu, C., Yang, M., 2019. Experimental and theoretical studies of a novel electrochemical sensor based on molecularly imprinted polymer and B, N, F-CQDs/AgNPs for enhanced specific identification and dual signal amplification in highly selective and ultra-trace bisphenol S determination in plastic products. Anal. Chim. Acta 1066, 36–48.
Zhang, H., Zhang, Y., Li, J., Yang, M., 2019a. Occurrence and exposure assessment of bisphenol analogues in source water and drinking water in China. Sci. Total Environ. 655, 607–613.
Zhang, J., Chen, Y., Wu, W., Wang, Z., Chu, Y., Chen, X., 2019b. Hollow porous dummy molecularly imprinted polymer as a sorbent of solid-phase extraction combined with accelerated solvent extraction for determination of eight bisphenols in plastic products. Microchem. J. 145, 1176–1184.
Zhang, X., Li, G., Wu, D., Zhang, B., Hu, N., Wang, H., Liu, J., Wu, Y., 2019c. Recent advances in the construction of functionalized covalent organic frameworks and their applications to sensing. Biosens. Bioelectron. 145, 111699.
Zhao, F., Liu, H., Mathe, S.D.R., Dong, A., Zhang, J., 2017. Covalent organic frameworks: from materials design to biomedical application. Nanomaterials-Basel 8, 15.
Zheng, Z., Liu, J., Wang, M., Cao, Juqing, Li, L., Wang, C., Feng, N., 2016. Selective sensing of bisphenol A and bisphenol S on platinum/poly(diallyl dimethyl ammonium chloride)-diamond powder hybrid modified glassy carbon electrode. J. Electrochem. Soc. 163, 192–199.
Zhou, J., Chen, X.H., Pan, S.D., Wang, J.L., Zheng, Y.B., Xu, J.J., Zhao, Y.G., Cai, Z.X., Jin, M.C., 2019. Contamination status of bisphenol A and its analogues (bisphenol S, F and B) in foodstuffs and the implications for dietary exposure on adult residents in Zhejiang Province. Food Chem. 294, 160–170.
Zhou, Q., Jin, Z., Li, J., Wang, B., Wei, X., Chen, J., 2018. A novel air-assisted liquid-liquid microextraction based on in-situ phase separation for the HPLC determination of bisphenols migration from disposable lunch boxes to contacting water. Talanta 189, 116–121.
Zhu, L., Cao, Y., Cao, G., 2014. Electrochemical sensor based on magnetic molecularly imprinted nanoparticles at surfactant modified magnetic electrode for determination of bisphenol A. Biosens. Bioelectron. 54, 258–261.
Zhu, W., Yue, X., Duan, J., Zhang, Y., Zhang, W., Yu, S., Wang, Y., Zhang, D., Wang, J., 2016. Electrochemically co-reduced 3D GO-C_{60} nanoassembly as an efficient nanocatalyst for electrochemical detection of bisphenol S. Electrochim. Acta 188, 85–90.